

Metal-to-insulator transition in two-dimensional ferromagnetic monolayer induced by substrate

Can Qi(齐灿), Jun Hu(胡军)

Citation: Chin. Phys. B . 2018, 27(7): 077106. **doi:** 10.1088/1674-1056/27/7/077106

Journal homepage: http://cpb.iphy.ac.cn; http://iopscience.iop.org/cpb

What follows is a list of articles you may be interested in

Electric current-induced giant electroresistance in $La_{0.36}Pr_{0.265}Ca_{0.375}MnO_3$ thin films

Yinghui Sun(孙颖慧), Yonggang Zhao(赵永刚), Rongming Wang(王荣明)

Chin. Phys. B . 2017, 26(4): 047103. **doi:** 10.1088/1674-1056/26/4/047103

Electric current-induced giant electroresistance in $La_{0.36}Pr_{0.265}Ca_{0.375}MnO_3$ thin films

Yinghui Sun(孙颖慧), Yonggang Zhao(赵永刚), Rongming Wang(王荣明)

Chin. Phys. B . 2017, 26(4): 047103. **doi:** 10.1088/1674-1056/26/4/047103

Doping-driven orbital-selective Mott transition in multi-band Hubbard models with crystal field splitting

Yilin Wang(王义林), Li Huang(黄理), Liang Du(杜亮), Xi Dai(戴希)

Chin. Phys. B . 2016, 25(3): 037103. **doi:** 10.1088/1674-1056/25/3/037103

Dynamic resistive switching in a three-terminal device based on phase separated manganites

Wang Zhi-Qiang, Yan Zhi-Bo, Qin Ming-Hui, Gao Xing-Sen, Liu Jun-Ming

Chin. Phys. B . 2015, 24(3): 037101. **doi:** 10.1088/1674-1056/24/3/037101

Emergent reversible giant electroresistance in spacially confined $La_{0.325}Pr_{0.3}Ca_{0.375}MnO_3$ wires

Cui Li-Min, Li Jie, Wang Jia, Zhang Yu, Zheng Dong-Ning

Chin. Phys. B . 2014, 23(9): 097103. **doi:** 10.1088/1674-1056/23/9/097103

Metal-to-insulator transition in two-dimensional ferromagnetic monolayer induced by substrate*

Can Qi(齐灿)[1,2] and Jun Hu(胡军)[1,2,†]

[1] School of Physical Science and Technology, Soochow University, Suzhou 215006, China
[2] Jiangsu Key Laboratory of Thin Films, Soochow University, Suzhou 215006, China

(Received 19 March 2018; revised manuscript received 18 April 2018; published online 25 June 2018)

Two-dimensional (2D) ferromagnetic (FM) materials have great potential for applications in next-generation spintronic devices. Since most 2D FM materials come from van der Waals crystals, stabilizing them on a certain substrate without killing the ferromagnetism is still a challenge. Through systematic first-principles calculations, we proposed a new family of 2D FM materials which combines TaX (X = S, Se or Te) monolayer and Al_2O_3(0001) substrate. The TaX monolayers provide magnetic states and the Al_2O_3(0001) substrate stabilizes the former. Interestingly, the Al_2O_3(0001) substrate leads to a metal-to-insulator transition in the TaX monolayers and induces a band gap up to 303 meV. Our study paves the way to explore promising 2D FM materials for practical applications in spintronics devices.

Keywords: metal-to-insulator transition, two-dimensional monolayer, ferromagnetic material

PACS: 71.30.+h, 73.22.–f, 76.50.+g **DOI:** 10.1088/1674-1056/27/7/077106

1. Introduction

Since the discovery of graphene,[1–3] extensive interests in two-dimensional (2D) materials have been inspired. In recent years, a number of other 2D materials were discovered, such as honeycomb boron nitride,[4] layered transition metal dichalcogenides,[5] black phosphorus,[6] and Mexene.[7] The 2D materials exhibit a variety of intriguing electronic and magnetic properties such as quantum spin Hall effect,[8] valleytronics,[9] and ferromagnetism,[7] which make the 2D materials promising for wide applications in the next-generation of electronic and spintronic devices.

In 2D systems, it was believed that the long-range magnetic order is strongly suppressed by thermal fluctuations, according to the Mermin–Wagner theorem.[10] However, magnetic anisotropy can counteract these thermal fluctuations and enable the long-range magnetic order. Recently, the 2D ferromagnetism has been demonstrated in $Cr_2Ge_2Te_6$ and CrI_3 monolayers,[11,12] and the magnetic anisotropy comes from the anisotropic superexchange interaction and large spin–orbital coupling of the I atom.[13] However, the Curie temperature (T_C) of $Cr_2Ge_2Te_6$ and CrI_3 monolayers is quite low (< 60 K), which hampers the practical applications in spintronic devices at room temperature. $FeBr_3$ monolayer with the same crystal structure as that of CrI_3 was predicted to have higher $T_C \sim 150$ K,[14] but it is still far below the room temperature. Recently, VSe_2 monolayer was discovered to possess strong ferromagnetic (FM) ordering above room temperature.[15] Nevertheless, VSe_2 monolayer is metallic, which may cause extra energy dissipation of spintronic devices. Furthermore, all these materials belong to van der Waals crystals, so each monolayer is electronically saturated, which leads to weak interaction with the neighboring monolayers or substrate. For real applications, it is necessary to place the 2D FM materials on certain substrates, but the van der Waals interaction between the 2D FM materials and substrates makes the heterostructure unstable. Therefore, exploring new 2D FM materials which are semiconducting, have high T_C, and can chemically bind to a substrate is of both fundamental interest and application merit.

In this paper, we proposed a new family of 2D FM semiconductors combined with TaX (X = S, Se, or Te) monolayer and Al_2O_3(0001) substrate based on first-principles calculations. Analyses of the electronic structures reveal that the TaX monolayers are ferromagnetic with a spin moment of 3 μ_B and undergo a metal-to-insulator transition when they are placed on the Al_2O_3(0001) substrate. The induced band gaps are remarkable, ranging from 188 meV to 303 meV. Furthermore, the magnetic states near the Fermi energy are localized within the TaX monolayers and exhibit 100% spin polarization.

2. Computational details

To model the Al_2O_3(0001) substrate, we constructed a slab with 18 atomic layers (thickness of ~ 11 Å), along with a vacuum of 15 Å between adjacent slabs. Then we put a TaX (X = S, Se, or Te) monolayer on Al_2O_3(0001). The atomic structure and electronic properties were calculated with density functional theory (DFT) as implemented in the Vienna *ab-initio* simulation package.[16,17] The interaction be-

*Project supported by the National Natural Science Foundation of China (Grant No. 11574223), the Natural Science Foundation of Jiangsu Province, China (Grant No. BK20150303), and the Jiangsu Specially-Appointed Professor Program of Jiangsu Province, China.

†Corresponding author. E-mail: jhu@suda.edu.cn

© 2018 Chinese Physical Society and IOP Publishing Ltd

tween the valence electrons and ionic cores was described within the framework of the projector augmented wave (PAW) method.[18,19] The Perdew–Burke–Ernzerhof type generalized gradient approximation was used for the exchange–correlation potentials.[20] The energy cutoff for the plane wave basis expansion was set to 500 eV. The 2D Brillouin zone was sampled by a 27×27 k-grid mesh. The atomic positions were fully relaxed with a criterion that requires the force on each atom to be smaller than 0.01 eV/Å.

3. Results and discussion

As mentioned above, the VSe_2 monolayer is ferromagnetic with T_C above the room temperature. On the other hand, the spin–orbit coupling (SOC) leads to interesting phenomena in low-dimensional materials.[21] Therefore, we choose TaX_2 (X = S, Se or Te) monolayers (see Fig. 1(a)), which are the isovalent counterpart of the VSe_2 monolayer and the SOC effect of the Ta-5d orbital is much stronger than that of the V-3d orbital. However, the TaX_2 monolayers are electronically saturated, so it has only a van der Waals interaction with the substrate. To activate the chemical activity of the TaX_2 monolayers, we remove one anion layer, resulting in buckled honeycomb structure TaX monolayers, as shown in Fig. 1(b). Then we place the TaX monolayers on Al_2O_3(0001) substrate, as shown in Fig. 1(c). Here, we choose the Al_2O_3(0001) surface as the substrate, because it is widely used as the substrate to support low-dimensional materials in experiments.[22–24] Bulk Al_2O_3 is an insulator with a band gap of ∼ 9 eV, while the band gap of the Al_2O_3(0001) surface is reduced by about 1 eV due to the surface states.[25,26] From the density of states in Fig. 1(d), the calculated band gap of Al_2O_3(0001) is 4.6 eV, which is smaller than the experimental value but close to the previous theoretical calculation result.[27] It should be noticed that, in the experimental process of fabrication, the growth condition must be controlled delicately, so that the Ta layer grows on Al_2O_3(0001) first and then the X layer grows to form a honeycomb TaX monolayer.

We firstly study the properties of freestanding TaX monolayers. As listed in Table 1, the optimized lattice constant ranges from 3.1 Å to 3.3 Å. The Ta−Te bond length is significantly larger than the other two because of the larger atomic size of the Te atoms. The TaX monolayers keep buckling with buckling distances ranging from 1.65 Å to 2.00 Å, as listed in Table 1. All the TaX monolayers are magnetic and the magnetic moments are smaller than 1 μ_B. In addition, the magnetic moments increase slightly from TaS to TaTe, which may be attributed to the increasing lattice constants from TaS to TaTe. In addition, the TaX monolayers are metallic, as seen from the band structures in Fig. 2. For TaS and TaSe monolayers, there is a hole pocket at the M point in the majority spin channel, and an electron pocket between the M and Γ points in the minority spin channel. For the TaTe monolayer, the dispersions of the electronic bands near the Fermi energy (E_F) are much more complex than the other two cases, especially in the minority spin channel. Clearly, removing one anion layer from the TaX_2 monolayers induces spin polarization but retains the metallic character.[28,29]

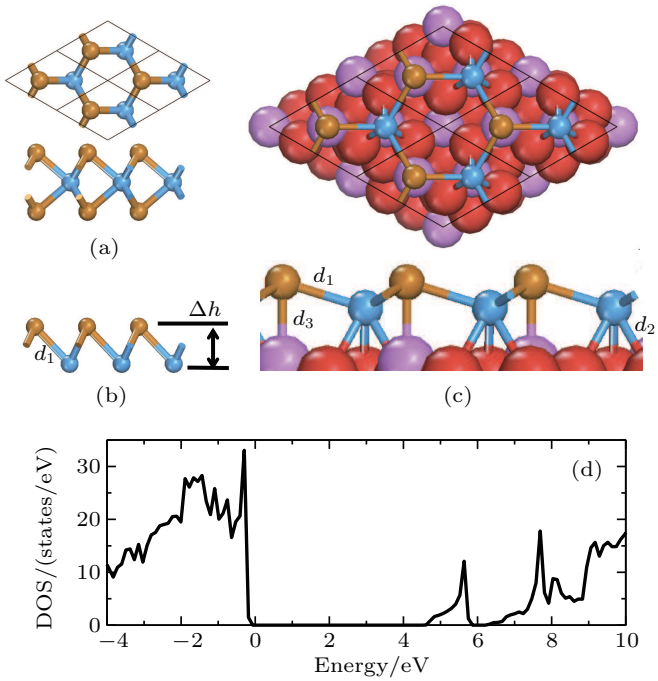


Fig. 1. (color online) The top view (top panels) and side view (bottom panels) of atomic structures of (a) TaX_2 monolayer, (b) TaX monolayer, and (c) TaX/Al_2O_3. The blue, brown, purple, and red spheres represent Ta, X (S, Se, or Te), Al, and O atoms, respectively. d_1, d_2, and d_3 denote the Ta–X, X–O, and Ta–Al bond lengths, respectively. Δh indicates the buckling distance of the TaX monolayer. (d) Density of states (DOS) of the Al_2O_3(0001) surface. The Fermi energy is set to be the zero point of energy.

Table 1. The magnetic moments (M_S in μ_B), Bader charges (ρ in e), and structural properties of freestanding and Al_2O_3(0001) supported TaX (X = S, Se, or Te) monolayers. a (in Å) indicates the lattice constant of the freestanding TaX monolayers. d_1, d_2, and d_3 (in Å) denote the Ta–X, X–O, and Ta–Al bond lengths, respectively, as marked in Fig. 1. The lattice constants are adjusted to match those of Al_2O_3(0001) (4.76 Å) when the TaX monolayers are placed on the substrate. The binding energy (E_b in eV) between the TaX monolayer and Al_2O_3(0001) is defined as $E_b = E(\mathrm{Ta}X) + E(\mathrm{Sub}) - E(\mathrm{Ta}X/\mathrm{Sub})$, where $E(\mathrm{Ta}X)$, $E(\mathrm{Sub})$, and $E(\mathrm{Ta}X/\mathrm{Sub})$ are the total energies of freestanding TaX, pure Al_2O_3(0001) substrate, and the combined system, respectively.

	Free standing						On substrate							
	a	d_1	Δh	M_S	ρ_{Ta}	ρ_X	d_1	d_2	d_3	Δh	M_S	E_b	ρ_{Ta}	ρ_X
TaS	3.10	2.43	1.65	0.88	–0.77	0.77	2.97	2.29	2.17	1.08	3	2.13	–1.33	1.56
TaSe	3.16	2.57	1.81	0.90	–0.61	0.61	3.02	2.29	2.32	1.25	3	1.88	–1.26	1.48
TaTe	3.31	2.77	2.00	0.94	–0.37	0.37	3.11	2.30	2.55	1.48	3	1.94	–1.16	1.36

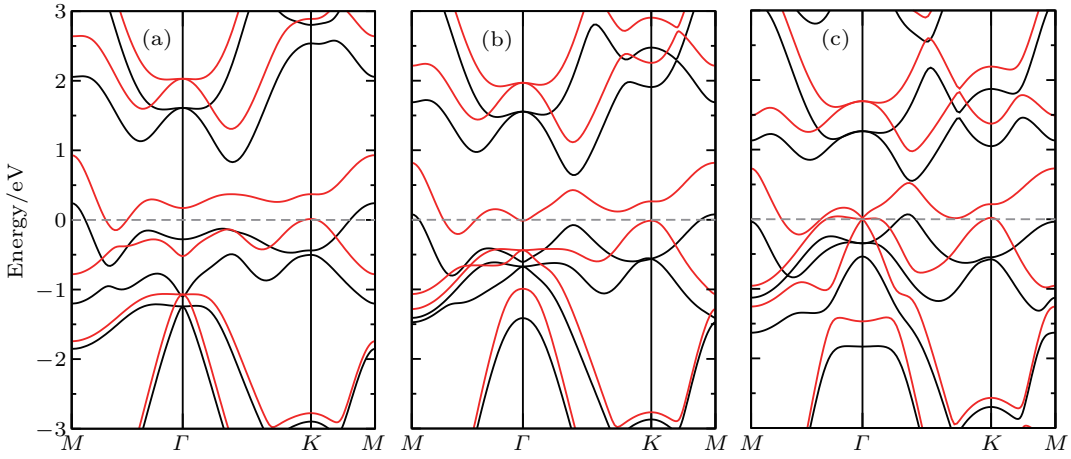


Fig. 2. (color online) Band structures of freestanding (a) TaS, (b) TaSe, and (c) TaTe monolayers. The black and red curves stand for bands in majority and minority spin channels, respectively. The horizontal dashed lines indicate the Fermi energy.

When the TaX monolayers are placed on $Al_2O_3(0001)$, the Ta atoms prefer the hollow sites comprised of three surface O atoms and the anion X atoms take the atop sites of the surface Al atoms, as shown in Fig. 1(c). Note that the lattice constant of $Al_2O_3(0001)$ (4.76 Å) is much larger than that of the freestanding TaX monolayers, so the substrate imposes a large extensive constraint on the TaX monolayers. Consequently, the Ta–X bond lengths increase significantly, and the buckling distances decrease obviously, as listed in Table 1. The Ta atoms bind strongly to the surface O atoms of $Al_2O_3(0001)$, with short Ta–O bonds ($\sim$ 2.3 Å). In addition, the interactions between the anion X atoms and Al atoms are also quite strong, resulting in short X–Al bonds ranging from 2.17 Å to 2.55 Å. Obviously, the TaX monolayers are chemically stuck on the $Al_2O_3(0001)$ substrate, which results in large binding energies around 2 eV as listed in Table 1. Therefore, the TaX monolayers are stable on the $Al_2O_3(0001)$ substrate, and the combined system TaX/$Al_2O_3(0001)$ could be regarded as an entire entity with the 2D FM states existing on the topmost layer.

It is instructive to see how the electronic and magnetic properties are modified by the $Al_2O_3(0001)$ substrate. Firstly, we find that the magnetic moment increases to 3 μ_B for all cases, similar to the phenomenon found in other materials with epitaxial strain from the substrate.[30,31] This can be attributed to the significant changes of the charge states of the Ta and X atoms as shown in Table 1. Clearly, based on the Bader charge division scheme,[32] the Ta atoms loose more electrons and the X atoms gain more electrons compared to the situation in the freestanding monolayers. Consequently, the change of charge states leads to the change of magnetic states.[33] Furthermore, the spin moments are mainly contributed by the Ta atoms, so the spin density distributes almost completely around the Ta atoms, as shown for the case of the TaTe/$Al_2O_3(0001)$ in Fig. 3(a).

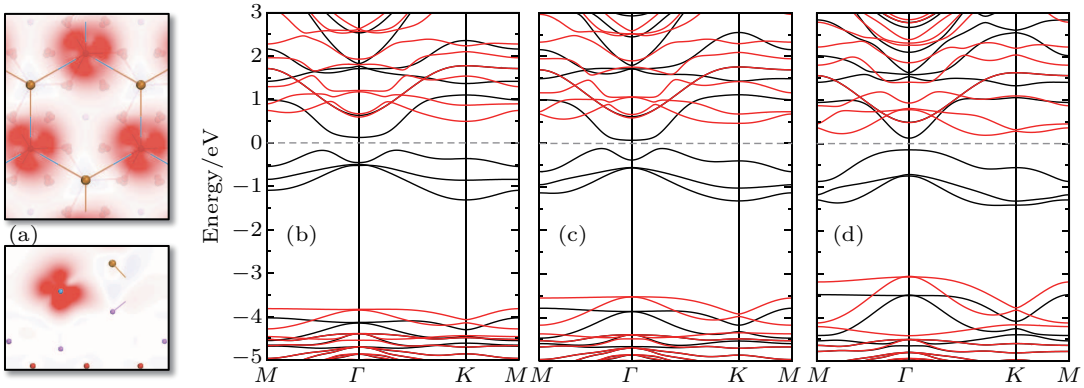


Fig. 3. (color online) (a) Spin density of TaTe/$Al_2O_3(0001)$ with cutoff of ± 0.3 e/Å^3. Top panel: parallel to the surface and crossing the Ta atoms; bottom panel: perpendicular to the TaTe monolayer and crossing one of the Ta–Te bonds. (b)–(d) Band structures of (a) TaS/$Al_2O_3(0001)$, (b) TaSe/$Al_2O_3(0001)$, and (c) TaTe/$Al_2O_3(0001)$. The black and red curves stand for bands in majority and minority spin channels, respectively. The horizontal dashed lines indicate the Fermi energy.

Interestingly, all the TaX/$Al_2O_3(0001)$ become semiconductors, as shown by the band structures in Figs. 3(b)–3(d), which indicates that metal-to-insulator transition is induced by the substrate. The band gaps are quite remarkable, 303.5 meV, 188.4 meV, and 235.4 meV for TaS/$Al_2O_3(0001)$, TaSe/$Al_2O_3(0001)$, and TaTe/$Al_2O_3(0001)$, respectively. The TaS/$Al_2O_3(0001)$ and TaSe/$Al_2O_3(0001)$ have indirect band gaps, while TaTe/$Al_2O_3(0001)$ is a direct-gap semiconductor.

This difference originates from the different sizes of the anion atoms, which result in different bond lengths and buckling distances as listed in Table 1. Furthermore, the bands near E_F are completely from the majority spin channel, while the valence bands in the minority spin channel are far below the E_F and bring about a large band gap in the minority spin channel. Therefore, the carriers excited by temperature or from doping exhibit 100% spin polarization.

To reveal the atomic-orbital contributions to the band structures, we plot the projected density of states (PDOS) of the Ta-5d orbitals and X-s and X-p orbitals in Fig. 4. Because of the local C_{3v} symmetry (see Fig. 1(c)), the d orbitals split into three groups: d_{xy/x^2-y^2}, $d_{xz/yz}$, and d_{z^2}, while the p orbitals split into two groups: $p_{x/y}$ and p_z. From Fig. 4, it can be seen that the states within 1.5 eV below the E_F in the majority spin channel are contributed from all components of the Ta-5d orbitals, only with little contributions from the anion atoms. The states from 0.5 eV to 2 eV above the E_F in the majority spin channel originate from d_{xy/x^2-y^2} and $d_{xz/yz}$, and are dominated by the latter. Similarly, the states from 0 eV to 3 eV in the minority spin channel are also contributed from the Ta-5d orbitals. This is understandable because the $Al_2O_3(0001)$ substrate is a wide-gap insulator, so its states are far way from E_F. Therefore, the spin current and electron current will localize within the TaX monolayers when the TaX/$Al_2O_3(0001)$ systems are used in spintronic devices. This is a good feature to keep the currents from contaminations caused by the substrate.

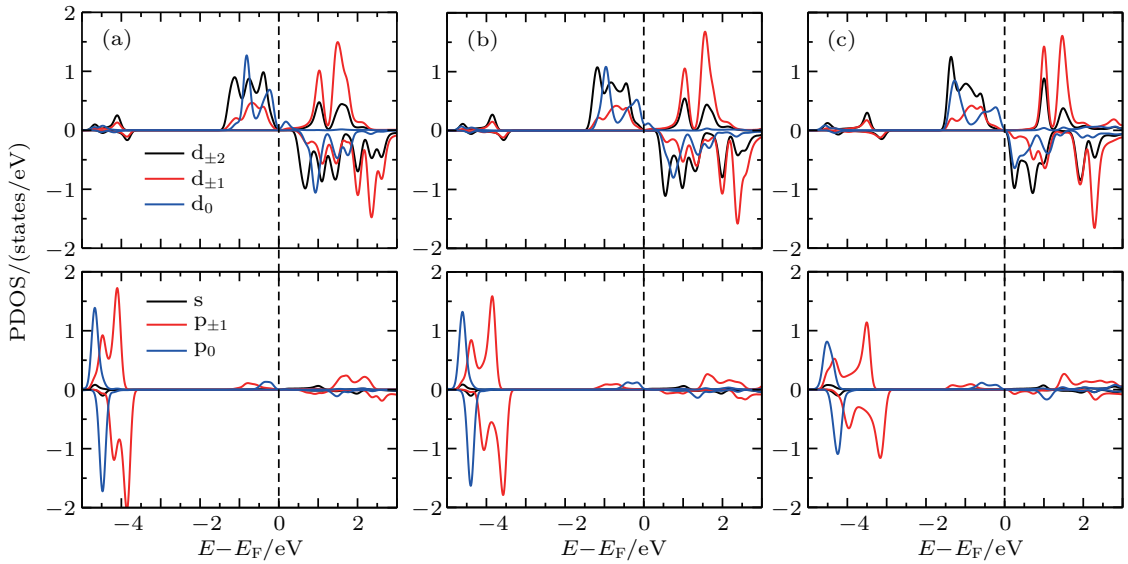


Fig. 4. (color online) Projected density of states (PDOS) on d orbitals of the Ta atom (top panels) and s and p orbitals of the anion atoms (bottom panels) for (a) TaS/$Al_2O_3(0001)$, (b) TaSe/$Al_2O_3(0001)$, and (c) TaTe/$Al_2O_3(0001)$. The vertical dashed lines indicate the Fermi energy. $d_{\pm2}$, $d_{\pm1}$, and d_0 stand for the $d_{xy+(x^2-y^2)}$, d_{xz+yz}, and d_{z^2} orbitals, respectively. $p_{\pm1}$ stands for the p_{x+y} orbital.

4. Conclusion

In summary, we investigated the electronic and magnetic properties of the TaX (X = S, Se or Te) monolayer in freestanding cases and supported by the $Al_2O_3(0001)$ substrate based on first-principles calculations. We found that both freestanding and substrate supported TaX monolayers are ferromagnetic. The TaX monolayers are chemically bound on the $Al_2O_3(0001)$ substrate with stable atomic structures. Interestingly, the freestanding TaX monolayers are metallic, while the substrate supported TaX monolayers are semiconductors with band gaps of 188–303 meV. Since the $Al_2O_3(0001)$ substrate is a wide-gap insulator, the states near the E_F are contributed by the TaX monolayers especially the Ta atom. Therefore, TaX/$Al_2O_3(0001)$ can be regarded as a 2D FM semiconductor. Our study paves the way to engineering 2D FM materials that are promising for practical applications in spintronics devices.

References

[1] Novoselov K S, Geim A K, Morozov S, Jiang D, Zhang Y, Dubonos S, Grigorieva I and Firsov A 2004 *Science* **306** 666
[2] Geim A K and Novoselov K S 2007 *Nat. Mater.* **6** 183
[3] Castro Neto A H, Guinea F, Peres N M R, Novoselov K S and Geim A K 2009 *Rev. Mod. Phys.* **81** 109
[4] Novoselov K, Jiang D, Schedin F, Booth T J, Khotkevich V V, Morozov S V and Geim A K 2005 *Proc. Natl. Acad. Sci. USA* **102** 10451
[5] Mak K F, Lee D, Hone J, Shan J and Heinz T F 2010 *Phys. Rev. Lett.* **105** 136805
[6] Li L K, Yu Y J, Ye G J, Ge Q Q, Qu X D, Wu H, Feng D L, Chen X H and Zhang Y B 2014 *Nat. Nanotechnol.* **9** 372
[7] Naguib M, Mochalin V N, Barsoum M W and Gogotsi 2014 *Adv. Mater.* **26** 992
[8] Kane C L and Mele E J 2005 *Phys. Rev. Lett.* **95** 146802
[9] Xu X D, Yao W, Xiao D and Heinz T F 2014 *Nat. Phys.* **10** 343
[10] Mermin N D and Wagner H 1966 *Phys. Rev. Lett.* **17** 1133
[11] Gong C, Li L, Li Z L, Ji H W, Stern A, Xia Y, Cao T, Bao W, Wang C Z, Wang Y, Qiu Z Q, Cava R J, Louie S G, Xia J and Zhang X 2017 *Nature* **546** 265
[12] Huang B, Clark G, Navarro-Moratalla E, Klein D R, Cheng R, Seyler K L, Zhong D, Schmidgall E, McGuire M A, Cobden D H, Yao W, Xiao D, Jarillo-Herrero P and Xu X D 2017 *Nature* **546** 270
[13] Lado J L and Fernández-Rossier J 2017 *2D Mater.* **4** 035002

[14] Zhang S H and Liu B G 2017 arXiv 1706.08943
[15] Bonilla M, Kolekar S, Ma Y, Diaz H C, Kalappattil V, Das R, Eggers T, Gutierrez H R, Phan M and Batzill M 2018 *Nat. Nanotechnol.* **13** 289
[16] Kresse G and Furthmüller J 1996 *Comput. Mater. Sci.* **6** 15
[17] Kresse G and Furthmüller J 1996 *Phys. Rev. B* **54** 11169
[18] Blöchl P E 1994 *Phys. Rev. B* **50** 17953
[19] Kresse G and Joubert D 1999 *Phys. Rev. B* **59** 1758
[20] Perdew J P, Burke K and Ernzerhof M 1996 *Phys. Rev. Lett.* **77** 3865
[21] Wu R Q and Freeman A J 1999 *J. Magn. Magn. Mater.* **200** 498
[22] Stierle A, Renner F, Streitel R, Dosch H, Drube W and Cowie B C 2004 *Science* **303** 1652
[23] Heinrich A J, Gupta J A, Lutz C P and Eigler D M 2004 *Science* **306** 466
[24] Kresse G, Schmid M, Napetschnig E, Shishkin M, Köhler L and Varga P 2005 *Science* **308** 1440
[25] Gautier M, Fenaud G, Van L P, Villette B, Pollak M, Thromat N, Jollet F and Duraud J P 1994 *J. Am. Ceram. Soc.* **77** 323
[26] Zhao G, Smith J, Raynolds J and Srolovitz D J 1996 *Interface Sci.* **3** 289
[27] Łodziana Z and Norskov J K 2001 *J. Chem. Phys.* **115** 11261
[28] Ding Y, Wang Y, Ni J, Shi L, Shi S and Tang W 2011 *Physica B* **406** 2254
[29] Manchanda P, Sharma V, Yu H B, Sellmyer D J and Skomski R 2015 *Appl. Phys. Lett.* **107** 032402
[30] Wei W G, Wang H, Zhang K, Liu H, Kou Y F, Chen J J, Du K, Zhu Y Y, Hou D L, Wu R Q, Yin L F and Shen J 2015 *Chin. Phys. Lett.* **32** 087504
[31] Bai Y H, Wang X, Mu L P and Xu X H 2016 *Chin. Phys. Lett.* **33** 087501
[32] Tang W, Sanville E and Henkelman G 2009 *J. Phys.: Condens. Matter* **21** 084204
[33] Masood H T, Muhammad Z, Habib M, Wang D M and Wang D L 2017 *Chin. Phys. B* **26** 067503